Science of the Total Environment 919 (2024) 170897

Contents lists available at ScienceDirect

Science of the Total Environment

journal homepage: www.elsevier.com/locate/scitotenv

A simple method for estimating the coarse lateral root biomass of shrubs using ground-penetrating radar: Validation by *Caragana microphylla* Lam. in Inner Mongolia

Luyun Zhang [a], Zheng Zhang [b], Li Guo [c], Xihong Cui [a,*], John R. Butnor [d], Shupeng Li [a], Xin Cao [a], Xuehong Chen [a]

[a] State Key Laboratory of Remote Sensing Science, Faculty of Geographical Science, Institute of Remote Sensing Science and Engineering, Beijing Normal University, Beijing 100875, China
[b] Key Laboratory of Ecological Warning, Protection & Restoration for Bohai Sea, Ministry of Natural Resources, North China Sea Environmental Monitoring Center, SOA, Qingdao 266033, China
[c] State Key Laboratory of Hydraulics and Mountain River Engineering, College of Water Resource and Hydropower, Sichuan University, Chengdu 610065, China
[d] USDA Forest Service, Northern Research Station, 81 Carrigan Drive, Aiken Center, University of Vermont, Burlington, VT, USA

HIGHLIGHTS

- Root counts can efficiently estimate the coarse lateral root biomass of shrubs.
- GPR is an efficient and labor-saving tool to obtain root counts.
- A proposed index R_a can summarize the characteristics of all detectable roots.
- The proposed method has the potential to be used in large regions.

GRAPHICAL ABSTRACT

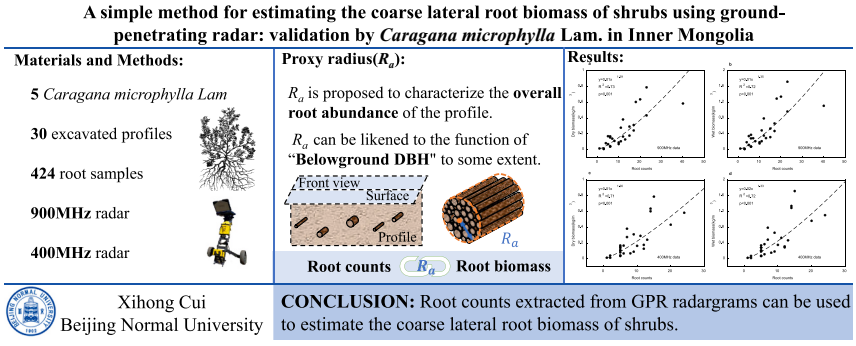

ARTICLE INFO

Guest Editor: Qinxue Wang

Keywords:
Ground-penetrating radar
Shrub root system
Root biomass
Root counts

ABSTRACT

The potential increases in carbon stocks in arid regions due to recent shrub encroachment have attracted extensive interest among both ecologists and carbon policy analysts. Quantifying the shrub root biomass amount in these ecosystems is essential to understanding the ecological changes occurring. In this paper, we proposed a simple nondestructive method for estimating the coarse lateral root biomass of shrubs based on the root counts obtained from ground-penetrating radar (GPR) radargrams. Root data were gathered via field experiments using GPR with antenna center frequencies of 900 MHz and 400 MHz. Five *Caragana microphylla* Lam. shrubs of different sizes were selected for measuring objects, and a total of 40 GPR survey lines were established for GPR data acquisition. The soil profile wall excavation method was used to obtain the total root biomass from each radargram. A model for estimating the root biomass was built by establishing the relationship between the root biomass in each profile and the root counts interpreted from the radargrams. According to the mathematical

* Corresponding author.
E-mail address: cuixihong@bnu.edu.cn (X. Cui).

https://doi.org/10.1016/j.scitotenv.2024.170897
Received 10 February 2023; Received in revised form 8 February 2024; Accepted 9 February 2024
Available online 10 February 2024
0048-9697/© 2024 Elsevier B.V. All rights reserved.

relationship between the root diameter and root biomass, the proxy root radius was derived, which could explain the rationality of the proposed model from the biological mechanism. The established model provided high confidence in estimating the root dry biomass using the GPR data obtained at the two antenna frequencies (R^2= 0.73 for 900 MHz and R^2= 0.71 for 400 MHz). The leave-one-out cross-validation results showed that the model exhibits satisfactory performance. This study expands the application of geophysical methods in root research and offers a new simplified method for estimating the root biomass from GPR data under field conditions.

1. Introduction

The root biomass and its belowground distribution are vital to understanding the global carbon cycle and sequestration in the terrestrial ecosystem and have become of longstanding interest to ecologists (Dean et al., 2015). Root production provides the primary input of organic carbon to soils (Raich and Nadelhoffer, 1989). Roots in arid and semiarid regions may comprise a substantial proportion of the total biomass in grassland ecosystems (Hu et al., 2019). According to the Food and Agriculture Organization (FAO), >18 % of the global land surface is covered by semiarid areas (Sjoholm et al., 1989), and such large areas provide carbon sequestration in these regions global significance (Brovkin et al., 2013). Moreover, quantifying the belowground biomass is essential for monitoring and assessing the degradation status in semiarid regions (Baumann, 2009; Liu et al., 2003; Zhou et al., 2022). However, our knowledge of plant roots is limited despite their essential role because they typically lie below the soil surface (Canadell et al., 1996).

Traditional techniques for measuring the root biomass are based on manual or mechanical excavations. These methods are accurate but laborious, destructive, difficult to implement, and only practical in small areas (Alamusa and Pei, 2003; Wang et al., 2008). Fortunately, the successful application of the ground-penetrating radar (GPR) in the detection of buried roots has provided a method for estimating the buried root biomass (Barton and Montagu, 2004; Butnor et al., 2012; Butnor et al., 2003; Butnor et al., 2001; Cui et al., 2019; Guo et al., 2013a; Hruska et al., 1999; Liu et al., 2019; Stover et al., 2007; Zhou et al., 2022). GPR employs electromagnetic waves to image the subsurface, relying on the principle of differential reflection. When the transmitting antenna emits electromagnetic waves, they encounter interfaces between materials with contrasting dielectric properties. These encounters cause partial reflection of the waves, with differences in reflection strength and travel time revealing the depth and location of underground features (Daniels, 2004). Data acquisition using GPR consists of collecting individual signal waveforms, known as A-scans, at specific points. By sequentially acquiring multiple A-scans along a survey line, a two-dimensional data set called a B-scan is generated. The B-scans can be visualized as grayscale images, termed radar profiles, where darker areas signify stronger reflections. Since roots possess distinct electrical properties compared to soil, their reflections manifest as hyperbolic shapes within B-scan profiles. For a comprehensive understanding of GPR principles and applications, please refer to the following recommended literature (Daniels, 2004; Guo et al., 2013a). The advantages of the GPR include the potential to monitor roots in large areas and to map the belowground root distribution (Guo et al., 2013a; Butnor et al., 2001; Hruska et al., 1999; Wu et al., 2014a, 2014b), as well as the repeatability of data collection facilitating time-series analysis.

Over the past 20 years, GPR technology, with antenna frequencies between 400 and 2000 MHz, has been evaluated as an effective technique for monitoring the underground coarse root system of plants (Čermák et al., 2000; Guo et al., 2013a; Stokes et al., 2002), and various methods to estimate the root biomass or diameter with the GPR have been developed (Barton and Montagu, 2004; Butnor et al., 2012; Butnor et al., 2003; Butnor et al., 2001; Cox et al., 2005; Cui et al., 2019; Dannoura et al., 2008; Guo et al., 2013a; Hirano et al., 2009; Hirano et al., 2012; Hruska et al., 1999; Stover et al., 2007). These methods have been used to predict the root biomass by extracting parameters related to the reflected signals of root objects from GPR data. These parameters can be summarized as A-scan waveform-based parameters (Barton and Montagu, 2004; Bi et al., 2023; Butnor et al., 2012; Cui et al., 2013; Dannoura et al., 2008; Guo et al., 2013a; Hirano et al., 2009; Hirano et al., 2012; Liang et al., 2021) and B-scan image-based parameters (Addo-Danso et al., 2016; Bain et al., 2017; Butnor et al., 2003; Butnor et al., 2001; Butnor et al., 2016; Cox et al., 2005; Dannoura et al., 2008; Hirano et al., 2009; Hirano et al., 2012; Molon et al., 2017; Sun et al., 2023).

A-scan waveform-based parameters, including the timing of phase changes (Barton and Montagu, 2004; Bi et al., 2023; Butnor et al., 2012; Cui et al., 2013; Guo et al., 2013a; Hirano et al., 2009; Hirano et al., 2012), the maximum amplitude value (Hirano et al., 2009; Hirano et al., 2012), and the maximum amplitude area (dB × ns) (Cui et al., 2013; Guo et al., 2013a; Hirano et al., 2009; Hirano et al., 2012; Liang et al., 2021; Yamase et al., 2018), are generally obtained by selecting A-scan data that pass through the middlemost position of the root from the processed B-scan images. This type of method enables accurate estimation of the root diameter or biomass when the root orientation is perpendicular to the direction of GPR measurement (Liu et al., 2018a; Tanikawa et al., 2013; Wang et al., 2020). Initial studies are mainly conducted under controlled experimental conditions where the root orientation is known. In recent years, Yamase et al. (2018) first used GPR waveform parameters to estimate the root diameter of mature *C. japonica* trees in weathered granite soils under forest field conditions. It has indicated that the sum of time intervals for all of the reflection waveforms was the only suitable parameter among the four proposed for estimating root diameter under forest field conditions. More studies are needed to clarify the suitability of the waveform-based parameters in different soil conditions and plant species in field condition.

B-scan image-based parameters can be extracted directly from GPR B-scan radargrams. The most common one is the area of the highly reflective region. GPR data are postprocessed, including position correction, background removal, Kirchhoff migration, and Hilbert transform. Then, the B-scan data are converted into 8-bit grayscale image files. An extraction threshold is set according to interpretation experience, and the number of high-amplitude pixels in the image above the set threshold is extracted. Finally, correlations are established between the number of pixels above the threshold and the root biomass (Butnor et al., 2016; Zhu et al., 2014). Butnor et al. (2001) first introduced this method and used it for estimating the root biomass at a depth of 40 cm. The correlation coefficient only reached 0.55 due to the surface environment and data processing methods. Butnor et al. (2003) used the same method to study the effectiveness of the GPR for estimating the root biomass in forest ecosystems. The results showed that this method could be employed to effectively assess the distribution and amount of the lateral root biomass and help reduce the number of soil cores to be sampled. This approach was also employed to estimate the belowground carbon stocks in a chronosequence of managed *Pinus palustris* stands, thus contributing to the development of whole ecosystem carbon accumulation models (Samuelson et al., 2014; Samuelson et al., 2017). Molon et al. (2017) used 1 GHz GPR to detect the root structure in a 400-m^2 white pine woodland and determined the coarse root biomass. In recent years, this method has been used in an increasing number of studies to estimate the root biomass (Addo-Danso et al., 2016; Alani and Lantini, 2019; Bain et al., 2017; Freschet et al., 2021; Liu et al., 2018b;

Sun et al., 2023).

Although the two types of GPR parameters have progressed in recent years, they still exhibit disadvantages. Both parameters require a complex processing process. The more complex the processing procedure is, the larger the possible error between the final extracted and original information. These methods are also operator intensive and challenging to automate without expert user guidance. Therefore, the workload of data processing and parameter extraction can be significant for root measurement and biomass estimation over large areas. Furthermore, these methods use the signal strength of the root reflected to estimate root biomass and assume that other complex influencing factors can be ignored. In practice, site characteristics, such as the soil texture and water content (Grote et al., 2003; Huisman et al., 2003), root size, root depth (Hirano et al., 2009), root orientation (Wang et al., 2020), and root water content (Guo et al., 2013b; Liu et al., 2018a), all impose a significant effect on the signal strength. Therefore, there is considerable uncertainty in estimating the root biomass using the signal strength, which is the main reason for the low accuracy obtained in field experiments.

Previous studies have shown that the significant advantage of the GPR in root research lies in identifying and localizing root objects (Wu et al., 2014a). In other words, the number and distribution of coarse roots can be obtained quickly and accurately by interpreting the GPR radargram. In this sense, a GPR radargram is analogous to a soil profile used in traditional root measurement methods for profile walls. In the traditional method, the number and spatial distribution of roots observed in the trench wall are important parameters in root ecological research (Bartos and Sims, 1974; Schafer and Nielsen, 1981). The point density of root intersections is converted into an estimate of the root length density based on empirical correlations or root anisotropy estimates (Chopart et al., 2008). Root counts in the profile could also be used to evaluate the root abundance in soil (Bartos and Sims, 1974). Schafer and Nielsen (1981) proposed a geometric model to calculate the root weight from root counts obtained in the excavated soil profile, and they suggested that root counts could be valuable for quickly assessing the root biomass in the field. However, the sampling process is time consuming, laborious, and destructive, making the observation of the number and spatial distribution of roots in the profile difficult, despite their importance. Fortunately, GPR technology can provide root counts (the number of roots identified in radargrams) in measured profiles quickly, easily, and nondestructively. Moreover, with a proper experimental setup, GPR technology can be used for root detection on a large quadrat or population scale.

Therefore, the aim of this study is to verify whether the root counts in a large area detected by GPR can be used to estimate the total coarse lateral root biomass within this range. Then, a simple model to estimate the root biomass on large spatial scales is constructed to address existing problems. It is assumed that (i) there may be a parameter analogous to the diameter at the breast height (DBH) that can be used to estimate the total biomass of all roots in a large area, (ii) the parameter may be correlated with the root counts within the range to be estimated, and (iii) the total biomass of coarse lateral roots within this range can be estimated from the root counts detected by the GPR. To achieve this, we first build a theoretical model based on GPR measurement scenarios and then validate the model by designing a coarse root detection experiment in the field. *Caragana microphylla* Lam., a typical shrub growing in the semiarid grasslands in Inner Mongolia, North China, was adopted as the research object.

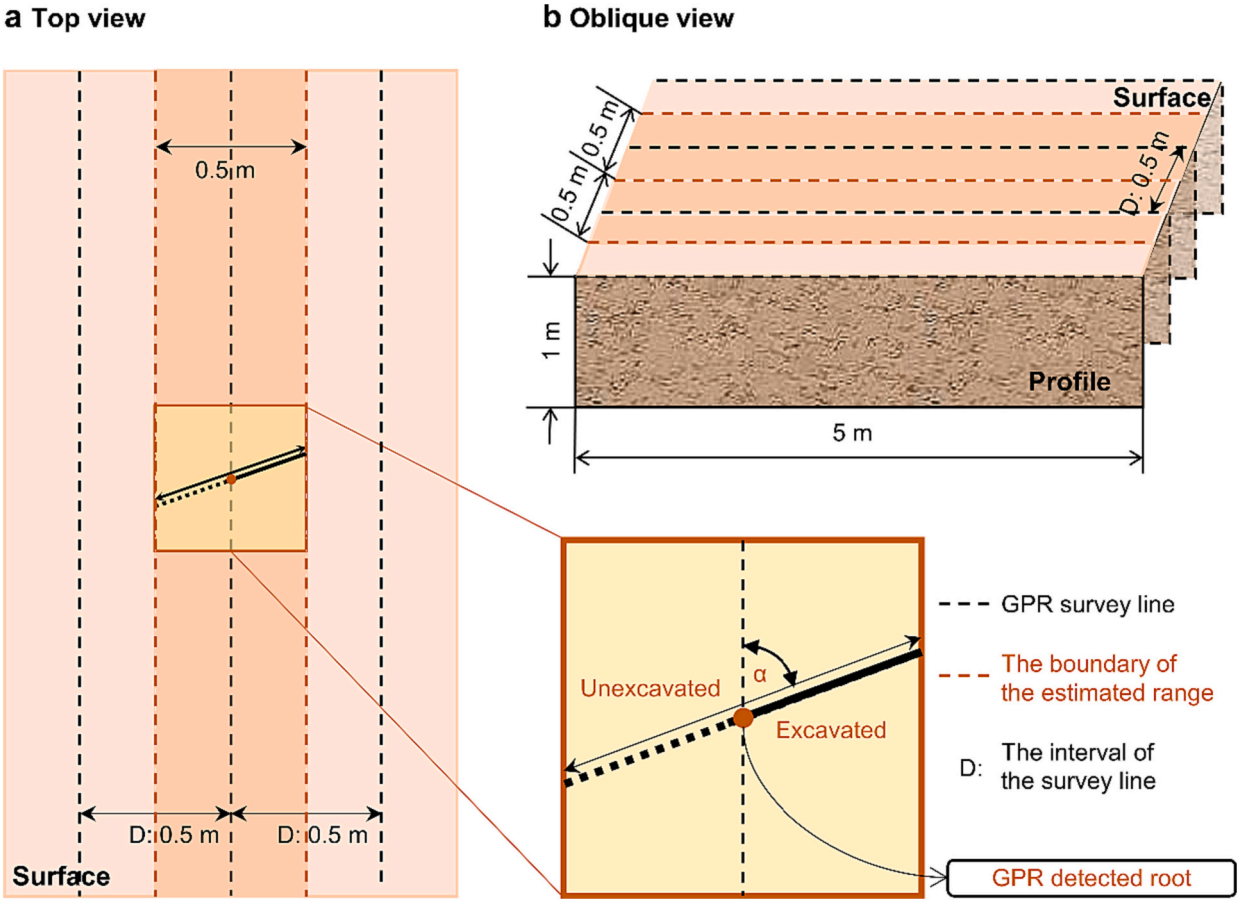

Fig. 1. **a** The schematic diagram of the field experiment from the top view. **b** The schematic diagram of the field experiment from the oblique view.

2. Materials and methods

2.1. Theoretical model establishment

GPR detection of the root system is generally achieved by a series of survey lines. The space detected by the GPR is directly related to the interval of the survey lines. Fig. 1 shows this concept from both top and oblique views. Under ideal conditions, the root is perpendicular to the profile along the horizontal and vertical directions, and the root length should match the spacing of the survey lines, which is assumed as 0.5 m here. A survey line can represent the condition of roots in a theoretical soil volume of $5 \times 0.5 \times 1m^3$. To reduce the differences due to the root length and orientation and to unify the study criteria, the root biomass was converted into the biomass per unit volume as the dependent variable according to the dimensions of the GPR profiles. Therefore, the volumetric root biomass can be calculated as follows:

$$B_i^{the} = \frac{\pi r_i^2 \rho_i D}{sin\alpha_i} \quad (1)$$

where B_i^{the} is the theoretical biomass of the i^{th} root. r_i is the radius of the i^{th} root, D is the interval of the survey line, ρ_i is the density of the i^{th} root (both the dry density and the wet density are acceptable), and α_i is the orientation of the i^{th} root. If there are n coarse roots in the theoretical volume (Fig. 2), the total root biomass in this theoretical volume can be expanded as:

$$B^{the} = \sum_{i=1}^{n} \frac{\pi r_i^2 \rho_i D}{sin\alpha_i} = \frac{\pi \rho_1 D}{sin\alpha_1} r_1^2 + \frac{\pi \rho_2 D}{sin\alpha_2} r_2^2 + \cdots + \frac{\pi \rho_n D}{sin\alpha_n} r_n^2 \quad (2)$$

In Eq. (2), each root exhibits a different orientation and density. B^{the} is the total biomass of roots in the theoretical volume corresponding to a survey line.

According to existing research and statistical results for actual measurements, the root density ρ of the same species at the same location can be considered the same (Cui et al., 2011). Therefore, considering n roots in the soil profile (Fig. 2), and assuming: $\rho_1 = \rho_2 = \cdots \rho_n = \rho$and $\alpha_1 = \alpha_2 = \cdots = \alpha_n = \alpha$, the Eq. (2) can be simplified as follows:

$$B^{the} = \frac{\pi \rho D}{\sin\alpha} \left(r_1^2 + r_2^2 + \cdots + r_n^2\right) = k\left(r_1^2 + r_2^2 + \cdots + r_n^2\right) \quad (3)$$

where k is a constant term, and D is the interval of the survey line. If D is fixed, k is mainly related to the root density. Eq. (3) indicates that the root biomass in the profile can be calculated as the sum of the biomass of each root. An index, R_a, is proposed to represent the characteristics of all detectable roots. This index is related to the radii of all detectable roots and can be regarded as the proxy radius of all roots, which can be obtained with Eq. (4):

$$R_a = \sqrt{r_1^2 + r_2^2 + \cdots + r_n^2} \quad (4)$$

Then, Eq. (3) can be expressed as:

$$B^{the} = kR_a^2 \quad (5)$$

where B^{the} is the total root biomass in the profile. The ecological implications are shown in Fig. 2b. R_a is particularly related to the number and diameter of roots. Regarding the existing root detection methods, it is difficult to obtain and calculate the proxy radius R_a directly. If R_a exhibits a stable relationship with the root counts n, the total root biomass in the profile can be expressed as Eq. (6):

$$B^{the} \propto R_a \propto n \quad (6)$$

This indicates that the total root biomass in the profile can be derived from the root count. The GPR provides a notable advantage in obtaining root counts from radar profiles (Wu et al., 2014a), so an empirical model linking the root biomass to the root counts detected by the GPR can be developed.

2.2. Field experiment

2.2.1. Study site

The study site (43°54′58″ N, 116°12′16″ E) occurs at the center of the Xilin Gol, Inner Mongolia, North China (Fig. 3). The average altitude of this area is 988.5 m, and this region is affected by a temperate continental climate. The annual average temperature in this area is 2.6 °C, involving four distinct seasons, with high temperatures occurring from June to August (Yiruhan et al., 2011). It is the most typical arid and semiarid area on the Mongolian Plateau, the annual potential evapotranspiration and the annual average precipitation are ~1750 and ~350 mm respectively (Miao et al., 2009), and the majority of the annual precipitation falls in July and August (He, 2012).

The soil types in this region are Calcic Chernozems and Calcic Orthic Aridisol, according to the FAO and the United States Department of Agriculture (USDA) soil classification systems, respectively (Li et al., 2013; WRB, 2006; Zhao et al., 2010). These soil types are mainly distributed in the eastern and central parts of the Mongolian Plateau, and the soil parent material is loess. This regional soil exhibits excessively drained characteristics, relatively homogeneous physiochemical properties, and low organic content, and is highly permeable, rendering it conducive to root detection with GPR (Cui et al., 2013; Li et al., 2016).

C. microphylla is the dominant shrub species in the study region. It exhibits high cold tolerance and drought tolerance, which determine its favorable position in a community competition (Cao et al., 2004). As a keystone species, *C. microphylla* largely controls the sequestration of organic carbon, nitrogen accumulation, and the hydrological cycle in this system (Cao et al., 2018).

2.2.2. GPR data collection

The experiment was conducted in October 2018, during which there was no rainfall (http://data.cma.cn/) and the weeds have wilted.

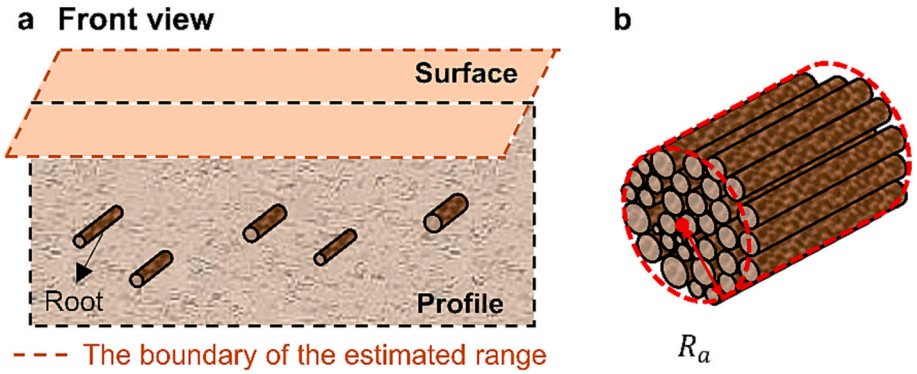

Fig. 2. **a** The front view of an excavated profile **b** The schematic diagram of the proxy radius R_a.

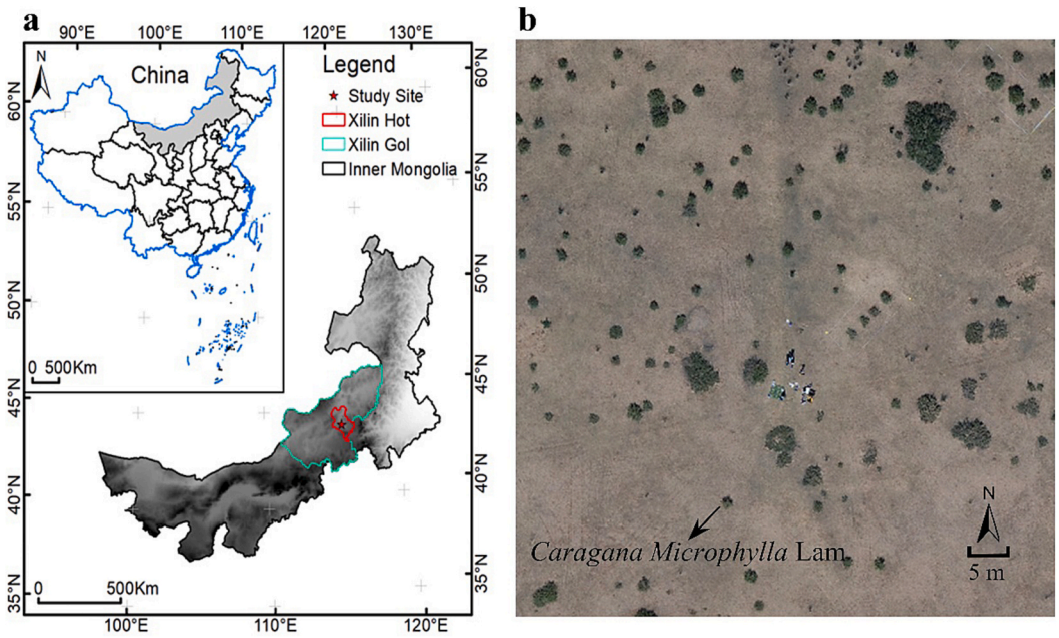

Fig. 3. **a** The study site is located in Xilin Hot, Inner Mongolia, China. **b** Unmanned aerial vehicle (UAV) image of the study site.

Considering the late timing of the experiment and the shallow weed root system, the influence of the weed roots on the experimental results was limited. The terrain of the experimental area is flat, and the ground angle is <3°. Five relatively isolated *C. microphylla* shrubs (with a distance from the stem to the nearest adjacent shrub stem larger than 4 m) were randomly selected for measurement to avoid interference from neighboring root systems (Fig. 4, Table 1). A total of 40 GPR survey lines with a 5-m length at every 0.5 m around the five shrubs were planned to observe the belowground root systems. The layout of the survey lines is shown in Fig. 4. To meet the modeling needs, the GPR detection area should contain different numbers, diameters, and degrees of sparseness of the distribution of the root system, so we chose different sizes of shrubs for measurement and set the direction of the survey line according to the root distribution of each shrub. We first conducted a preliminary survey of the area around the shrubs using the GPR to identify the area with a high root density. Then, in this area, the survey line was established with the shrub as the center. To avoid crossings, the lines were oriented along the same direction for each shrub and were as perpendicular to the lateral root orientation as possible. The layout of the survey lines shown in Fig. 4 represents the position relative to the target shrub surveyed, and not all lines were oriented along the same direction.

A field-portable GPR system (RIS MF Hi-Mod; Ingegneria Dei Sistemi Inc., Pisa, Italy) with two pairs of antennas shielded in the same antenna box was used to scan the shrub root system along the survey lines. The GPR system simultaneously collected data at two frequencies (900 and 400 MHz). An antenna box with a survey wheel was used to measure the electromagnetic pulses emanating from the GPR unit and record the survey distance. Each pulse was recorded as a trace comprising 512 samples with a time step of 0.0586 (or 0.1172) ns for a total record length of 40 (or 60) ns for the 900 (or 400) MHz antenna. The traces were triggered every 1.6 (or 3.2) cm for the 900 (or 400) MHz antenna along each survey line. In addition, a metal bar was buried in the soil at a depth of 30 cm, which was used to estimate the average velocity of the radar waves and calculate the depth of the detected roots (Cui et al., 2019; Liu et al., 2018b; Wu et al., 2014a).

2.2.3. Profile excavation

After GPR measurement, trenches 5 m long, 0.5 m wider and 1 m deep were excavated vertically along the survey lines (Fig. 4). Based on the GPR results and the profile root conditions, it was decided whether the profile would be excavated considering the workload of profile excavation. Specifically, according to field manual interpretation, the profile was not excavated when there was excessive noise in the radargram and the root signal was polluted. Eventually, 30 transects 5 m long, 0.5 m wider and 1 m deep were excavated vertically along the survey lines and used to establish a root biomass estimation model, as shown in Fig. 4g. Steel tapes, vernier calipers, and protractors were used to measure the location, horizontal orientation, diameter, and other information of each exposed coarse root (a diameter larger than 0.2 cm) in the excavated profiles. For example, the excavated roots in the No. 108 profile are shown in Fig. 5b. Each root was cut to a 20-cm length in the section directly below the antenna travel trajectory as a root sample and used to measure the wet biomass. The number of roots in each profile was counted and recorded in situ. Then, these roots were transported to the laboratory and weighed after oven drying at 65 °C for 72 h to obtain the dry biomass. After recording the root data of each profile, the trenches were backfilled.

2.3. Data processing and analysis

2.3.1. GPR data processing

The GPR data were processed using the RGPR package written in R software (R Core Team, 2022), which is primarily used to process and visualize GPR data (Huber and Hans, 2018). The steps and purposes of GPR data processing can briefly be described as follows: (1) *first break correction* is used to correct the vertical and horizontal scales in the radargrams and to place all reflections under the correct two-way travel time; (2) *background removal* is used to remove the background noise or clutter caused by signal interference, multiple reflections of GPR signals, parallel bands and high-frequency spike events; (3) *bandpass wave filtering* is used to remove the high- and low-frequency noise in each profile; (4) *automatic gain control (AGC)* is used to compensate for the energy loss caused by medium attenuation, scattering losses, and dissipation; and (5) *travel time-to-depth conversion*, which is used to obtain the depth of belowground targets by the wave velocity calculated based on the predefined depth of the metal bar. A processed GPR radargram collected by the 900 MHz antenna for the No. 108 profile is shown in Fig. 5a. For the detailed processes of each step, readers are referred to Cui et al. (2011), and Guo et al. (2013a). After radar data processing, the

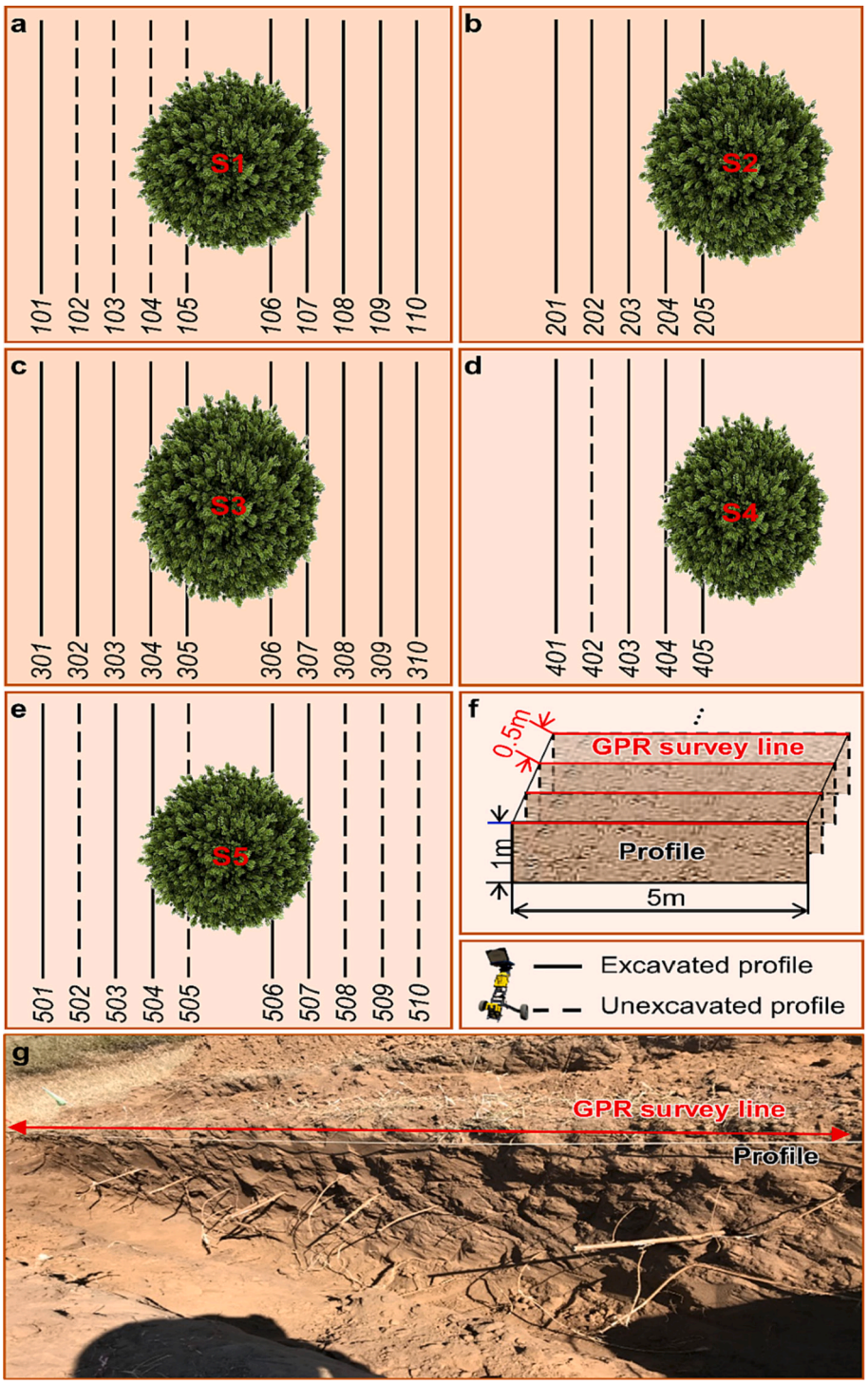

Fig. 4. Schematic diagram of field experiment data collection. **a** Survey lines of shrub S1; **b** Survey lines of shrub S2; **c** Survey lines of shrub S3; **d** Survey lines of shrub S4; **e** Survey lines of shrub S5; **f** A schematic of the profiles (5 m long, 1 m depth and arranged at 0.5 m intervals); **g** A photo of the excavated transects in the field experiment.

reflected signals from coarse roots exhibit a hyperbolic shape.

We used the enhanced YOLOv4 algorithm to automatically identify hyperbolic reflections and locate roots in the GPR images (Li et al., 2022). Thus, the root counts and locations within each profile could be automatically obtained. Then, the location of the roots identified in the radargram was automatically compared with that of the roots recorded along the excavated transects (Fig. 5b). Roots were considered accurately identified if the Euclidean distance between the root identified in the radargram and the root recorded along the profile was smaller than 15 cm. This value of 15 cm was determined based on the minimum spacing between the two roots that could be detected (Hirano et al., 2009). The detection rate is the ratio of the number of roots detected by GPR to the actual total number of roots on the profile (Hirano et al., 2012). It can be calculated using the formula: Detection rate (%) = (Root counts detected by GPR / Root counts measured) × 100 % (Table 2).

2.3.2. *Root biomass estimation model development*

The roots measured by the excavated profile method were used to

Table 1
Descriptive statistics of sampled individual *C. microphylla*.

Shrub no.	Long crown[a] (m)	Short crown[b] (m)	Crown width[c] (m)	Height (m)
S1	2.90	2.40	2.65	1.30
S2	3.50	2.70	3.10	1.05
S3	3.60	2.40	3.00	1.20
S4	2.20	1.80	2.00	1.25
S5	2.40	2.20	2.30	1.15

[a] The long crown is equal to the major axis of the crown of the shrub.
[b] The short crown is equal to the minor axis of the crown of the shrub.
[c] The crown width is equal to the average of the major and minor axis of the crown.

assess the rationality of the proxy radius of roots in the profile and to examine the relationship between the proxy radius and the number of roots. First, the proxy radius R_a of each excavated profile was calculated based on the root diameter recorded in the field according to Eq. (4), and the relationship between proxy radius R_a and root biomass on the profile was constructed. Second, proxy radius R_a against the root count in each profile to examine their relationship. Then, the relationship between the root biomass and root counts was further analyzed by using the relationship between the root biomass and proxy radius R_a (Eq. (5)). Finally, based on the above relationship, regression analysis was performed to develop an empirical model of the relationship between the root biomass and the root count in each GPR radargram. Regression analysis was performed in MATLAB software (The MathWorks, Inc., Natick, USA).

2.4. Model assessment and validation

2.4.1. Model assessment

The accuracy of the biomass model was evaluated based on a combination of five fit statistics: (i) coefficient of determination (R^2); (ii) correlation coefficient (r); (iii) root mean square error (RMSE); (iv) *p* value; (v) 1:1 line. R^2 characterizes the goodness of fit of the model. In other words, it provides a measure of the degree of agreement between the predicted and actual values. The correlation coefficient (r) is usually used to describe the degree of linear correlation between two variables. The root mean square error (RMSE) was used to evaluate the accuracy of the established model for estimating the root biomass.

$$R^2 = 1 - \frac{\sum_{j=1}^{m} (y_j - \hat{y}_j)^2}{\sum_{j=1}^{m} (y_j - \bar{y})^2} \tag{7}$$

$$r = \frac{\sum_{j=1}^{m} [(\hat{y}_j - \bar{\hat{y}}) \times (y_j - \bar{y})]}{\sqrt{\sum_{j=1}^{m} (\hat{y}_j - \bar{\hat{y}})^2} \times \sqrt{\sum_{j=1}^{m} (y_j - \bar{y})^2}} \tag{8}$$

$$RMSE = \frac{1}{m} \sqrt{\sum_{j=1}^{m} (y_j - \hat{y}_j)^2} \tag{9}$$

where m is the number of excavated profiles and y_j, $\hat{y}_j$ $\bar{y}$, and $\bar{\hat{y}}$ are the excavated, estimated, and average excavated root biomass values for the j^{th} profile and the average estimated root biomass, respectively.

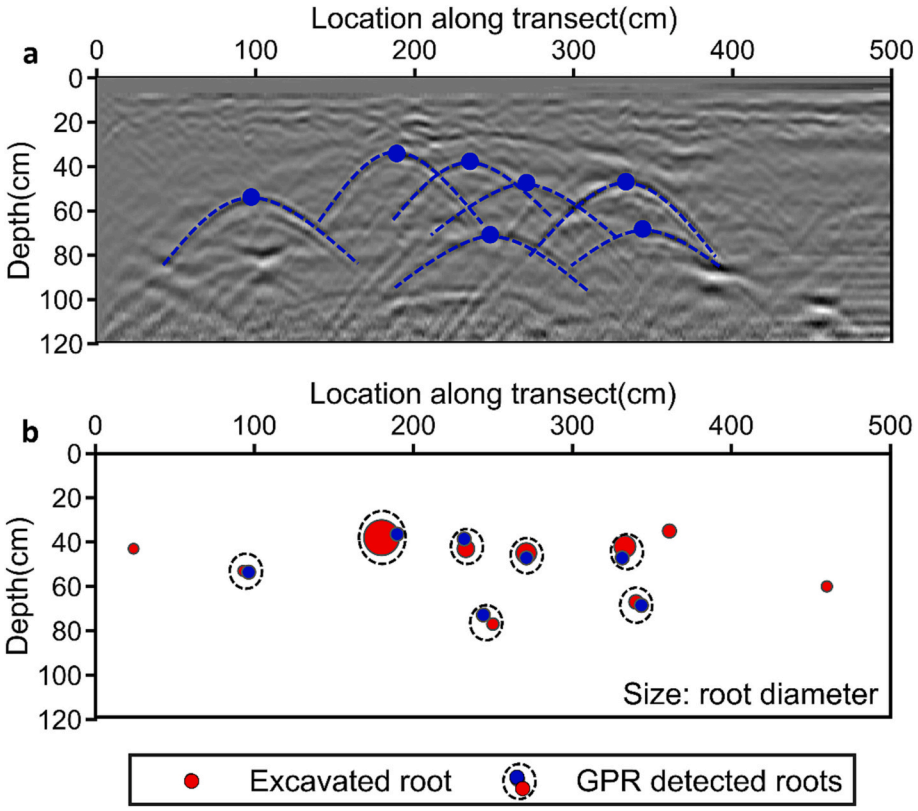

Fig. 5. **a** GPR radargram collected by the 900Mhz antenna for No. 108 profile. Blue points indicate the location of roots identified by GPR. **b** 900 MHz radar detected roots and excavated roots on the No. 108 profile. Red points indicate the location of excavated roots. The size of red point represents the root diameter. The black dotted circle represents the root detected by GPR.

Table 2
Total number and summary statistics of roots in each profile from excavation and GPR measurement.

Profile No.	Root counts measured	Root counts detected by GPR		GPR detection rate[a] (%)		R_a (cm)	Dry root biomass (kg/m^3)	Wet root biomass (kg/m^3)
		900 MHz	400 MHz	900 MHz	400 MHz			
101	3	3	0	100	0	0.40	0.01	0.01
106	12	8	5	67	42	1.40	0.11	0.21
107	18	15	12	83	67	1.23	0.18	0.32
108	10	7	5	70	50	1.06	0.14	0.29
109	8	6	5	75	63	0.51	0.04	0.07
110	4	3	2	75	50	0.42	0.01	0.02
201	13	10	9	77	69	1.07	0.09	0.19
202	8	5	5	63	63	1.20	0.17	0.34
203	22	17	9	77	41	1.91	0.31	0.66
204	21	17	13	81	62	1.89	0.24	0.47
205	44	40	24	91	55	3.02	0.58	1.11
301	7	6	6	86	86	1.33	0.17	0.37
302	12	12	10	100	83	1.68	0.17	0.35
303	28	23	20	82	71	2.41	0.43	0.97
304	30	23	15	77	50	2.71	0.79	1.72
305	22	20	14	91	64	3.17	0.64	1.34
306	21	18	14	86	67	3.00	0.60	1.29
307	15	12	7	80	47	2.02	0.38	0.79
308	15	13	12	87	80	1.49	0.13	0.29
309	11	10	8	91	73	1.13	0.07	0.16
310	8	4	5	50	63	1.55	0.08	0.19
401	1	0	0	0	0	0.14	0	0
403	1	1	1	100	100	0.50	0.01	0.03
404	7	6	5	86	71	0.81	0.04	0.08
405	13	11	5	85	38	1.39	0.11	0.21
501	6	0	2	0	33	0.75	0.04	0.08
503	11	5	6	45	55	0.89	0.07	0.12
504	10	6	5	60	50	1.01	0.15	0.29
506	24	15	11	63	46	2.76	0.29	0.53
507	19	11	7	58	37	1.10	0.28	0.49
Mean	14	11	8	78	60	1.47	0.21	0.43

[a] Detection rate (%) = 100 × (Root counts detected by GPR / Root counts measured).

2.4.2. Cross validation

Due to the small number of excavated profiles, leave-one-out cross-validation (LOO-CV) was applied to assess the biomass model accuracy. For a sample dataset with m samples, only one sample is selected for testing at a time, and the remaining $m-1$ samples are used for model construction. This process is repeated m times until the validation prediction values are obtained for all m samples (Geisser, 1974).

The percent bias (%), root mean squared error (RMSE, kg/m^3), root mean absolute error (MAE, kg/m^3) and coefficient of determination (R^2) were used to assess the model applicability. When the percent bias is positive, it indicates that the estimated value is on the high side, and vice versa. The *RMSE* was used to evaluate the prediction effect of the model; the smaller the value is, the better the prediction effect. When the MAE is equal to 0, the model is perfect. The larger the MAE is, the larger the model error. Models that produce small LOO-CV errors are preferred. The above metrics can be calculated as follows:

$$\text{Bias} = \frac{1}{m}\sum_{i=1}^{m}\frac{100}{n}\sum_{j=1}^{n}\frac{y_j - \hat{y}_j}{y_j} \tag{10}$$

$$\text{RMSE} = \frac{1}{m}\sum_{i=1}^{m}\sqrt{\frac{1}{n}\sum_{j=1}^{n}\left(y_j - \hat{y}_j\right)^2} \tag{11}$$

$$\text{MAE} = \frac{1}{m}\sum_{i=1}^{m}\frac{100}{n}\sum_{j=1}^{n}\left|y_j - \hat{y}_j\right| \tag{12}$$

where, m is the number of repetitions of the validation process, which is equal to the number of excavated profiles, and n is the number of profile samples per repetition, which is equal to $m-1$.

3. Results

3.1. Root and profile information

A total of 424 roots with diameters larger than 0.2 cm were measured by progressive excavation. Detailed information on the roots in each profile is provided in Table 2. The mean detection rates at the 900 MHz and 400 MHz radar frequencies over all profiles were 78 % and 60 %, respectively. Detection rates exceeding 60 % were observed in 86 % and 54 % of the profiles using the 900 MHz and 400 MHz antennas, respectively. The detection rate of the 900 MHz antenna is slightly higher than that of the 400 MHz antenna in most of the profiles. The distribution histograms of the dry density, wet density, radius, and orientation of all excavated roots are shown in Fig. 6. The dry and wet densities of the roots were normally distributed, with mean values of $0.52 g/cm^3$ and $1.00 g/cm^3$, respectively. The root radius showed an approximate power-law distribution. The mean root radius was 0.38 cm, and the maximum radius was 2.23 cm. Roots with a radius smaller than 0.5 cm accounted for 78 % of the total sample. The orientation of the roots was normally distributed, with an average orientation angle of 88°, and >89 % of the roots exhibited an orientation angle between 45° and 135°.

3.2. Relationship between the root biomass and the proxy radius

As shown in Fig. 7a and b, there is a power-law relationship between the proxy radius Ra and the excavated root biomass of each profile. The coefficient of determination for the dry biomass ($R^2 = 0.90$) was slightly lower than that for the wet biomass ($R^2 = 0.92$), indicating that the proxy radius Ra can be used to accurately estimate the root biomass (Fig. 7c and d, respectively). Compared with the theoretically derived results (Eq. (5)), the power index is 1.82 (for the dry biomass) and 1.91 (for the wet biomass), which is slightly <2, probably due to changes in

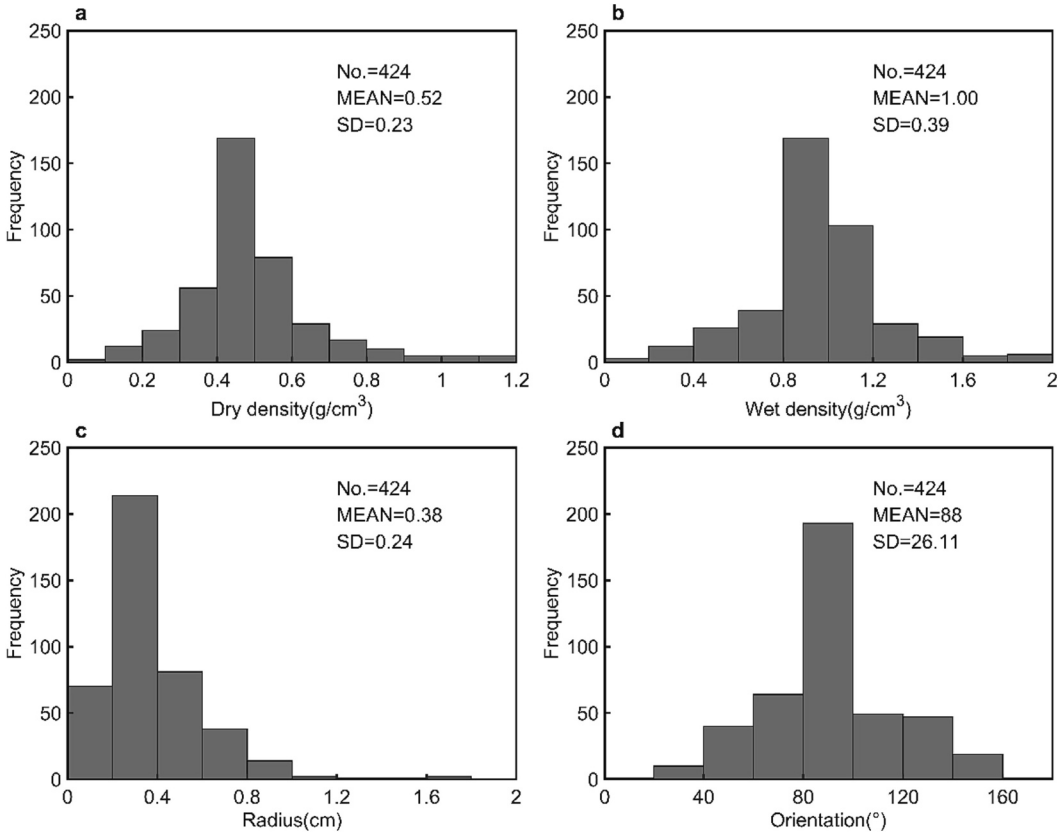

Fig. 6. **a** Distribution of root dry density (g/cm^3); **b** Distribution of root wet density (g/cm^3); **c** Distribution of root radius (cm); **d** Distribution of root orientation (°).

the density of roots with different radii (Fig. 6).

3.3. Validation of the theoretical model

Fig. 8a shows the relationship between the proxy radius R_a and the number of roots counted in the excavation profile. As previously hypothesized, the root count is strongly correlated with the proxy radius R_a, while there also exists a satisfactory power-law relationship between these variables in each soil profile ($y = 0.221x^{0.71}$, $R^2 = 0.79$, p-value < 0.001), which verifies the above conjecture in Section 2.1. Therefore, the relationship between proxy radius R_a and the root counts n can be expressed as:

$$R_a = mn^t \tag{13}$$

Substituting the Eq. (13) into the Eq. (5), the total root biomass in each profile can be expressed as:

$$B^{the} = k(mn^t)^2 = km^2n^{2t} = Kn^T \tag{14}$$

Eq. (14) shows that there is also a power-law relationship between the root biomass and root counts, which is verified in Fig. 8b and c. Across all 30 profiles, the root biomass increases exponentially with root counts (exponential regression, $R^2 = 0.83$, p value <0.001 for the dry biomass and 0.82 for the wet biomass). The results validate the theoretical model presented in Section 2.1.

3.4. Root biomass estimation using GPR data

The relationship statistics for the dry and wet biomass estimation models based on GPR data slightly differ. The regression relationships show similar R^2 and p values (<0.001). The dry biomass was closely related to the root counts identified from the 900 MHz radargrams with $R^2 = 0.73$, whereas the model based on the root counts identified from the 400 MHz radargrams yielded $R^2 = 0.71$. The models based on 900 and 400 MHz data achieves similar performance levels in estimating the root biomass.

3.5. Model validation results

Table 3 provides the model validation results for the measured data and the GPR data. The model based on the root counts obtained from the excavation method had a high R^2 value and produced the lowest bias, RMSE, and MAE values in estimating the root biomass. In comparison, the model based on the GPR data performed slightly worse. The use of the 900 MHz data to estimate the dry biomass provided a similar precision to that when using the 400 MHz data, with similar R^2 (0.73 vs. 0.71), RMSE (0.02 kg/m^3 vs. 0.02 kg/m^3), MAE (0.09 kg/m^3 vs. 0.10 kg/m^3) and bias (20.16 % vs. 16.64 %) values, even though the 900 MHz radar has a higher detection rate than the 400 MHz radar (78 % vs. 60 %, Table 2). Similar results were obtained when using the data at two frequencies to estimate the wet biomass. In summary, the root counts detected using the GPR can be used to effectively estimate the coarse lateral root biomass, and the performance levels of the two models based on the two antenna frequencies (900 and 400 MHz) are comparable.

4. Discussion

4.1. Significance of the root counts

Root counts are not utilized in many applications due to the difficulties of the data acquisition methods. However, as an advanced nondestructive geophysical detection technique, the GPR can efficiently, accurately, and nondestructively obtain the root count and the spatial distribution in each radar profile (Butnor et al., 2003), which offers the possibility of better utilizing this covariate in root system investigation. In this study, we used the root counts obtained from the GPR profile,

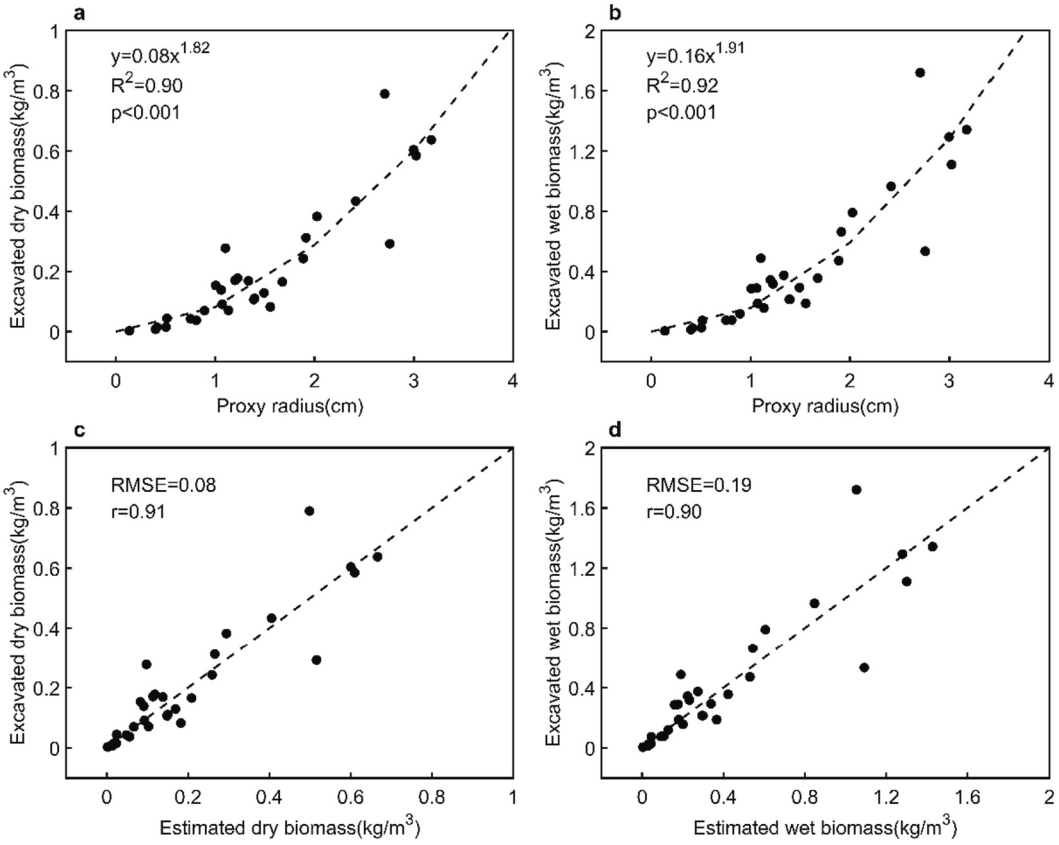

Fig. 7. **a** Correlation between proxy radius and root dry biomass; **b** Correlation between proxy radius and root wet biomass; **c** Plot of observed root dry biomass vs. estimated root dry biomass from proxy radius; **d** Plot of observed root wet biomass vs. estimated root wet biomass from proxy radius.

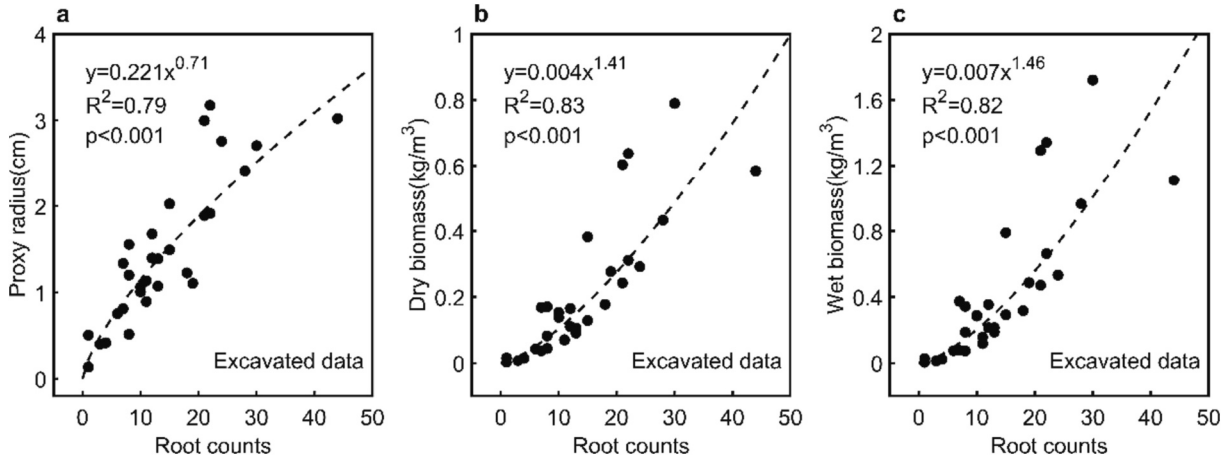

Fig. 8. **a** Correlation between root counts and proxy radius based on measured data; **b** Correlation between root counts and root dry biomass based on measured data; **c** Correlation between root counts and root wet biomass based on measured data.

Table 3
The result of cross-validation of biomass models.

Estimated variable	Data	Bias (%)	RMSE (kg/m^3)	MAE (kg/m^3)	R^2
Dry biomass	Measured	−13.86	0.01	0.08	0.83
	900 MHz	−20.16	0.02	0.09	0.73
	400 MHz	−16.64	0.02	0.10	0.71
Wet biomass	Measured	−16.44	0.08	0.17	0.82
	900 MHz	−22.78	0.09	0.19	0.73
	400 MHz	−17.72	0.09	0.21	0.72

rather than the root counts measured via the traditional profile wall method, to estimate the root biomass. Our results show that the root count data detected by GPR exhibit a favorable power-law relationship with the total root biomass in the range scanned by the GPR (Fig. 9). The biomass estimation model constructed based on this relationship can be used to estimate the coarse lateral root biomass of shrubs. In addition, the theoretical derivation of the proposed proxy radius R_a can explain the rationality of the model, which is consistent with our hypothesis and the results of other studies (Plaza-Bonilla et al., 2014).

Compared to existing parameters (A-scan waveform-based and B-scan image-based) for root biomass estimation extracted from GPR data,

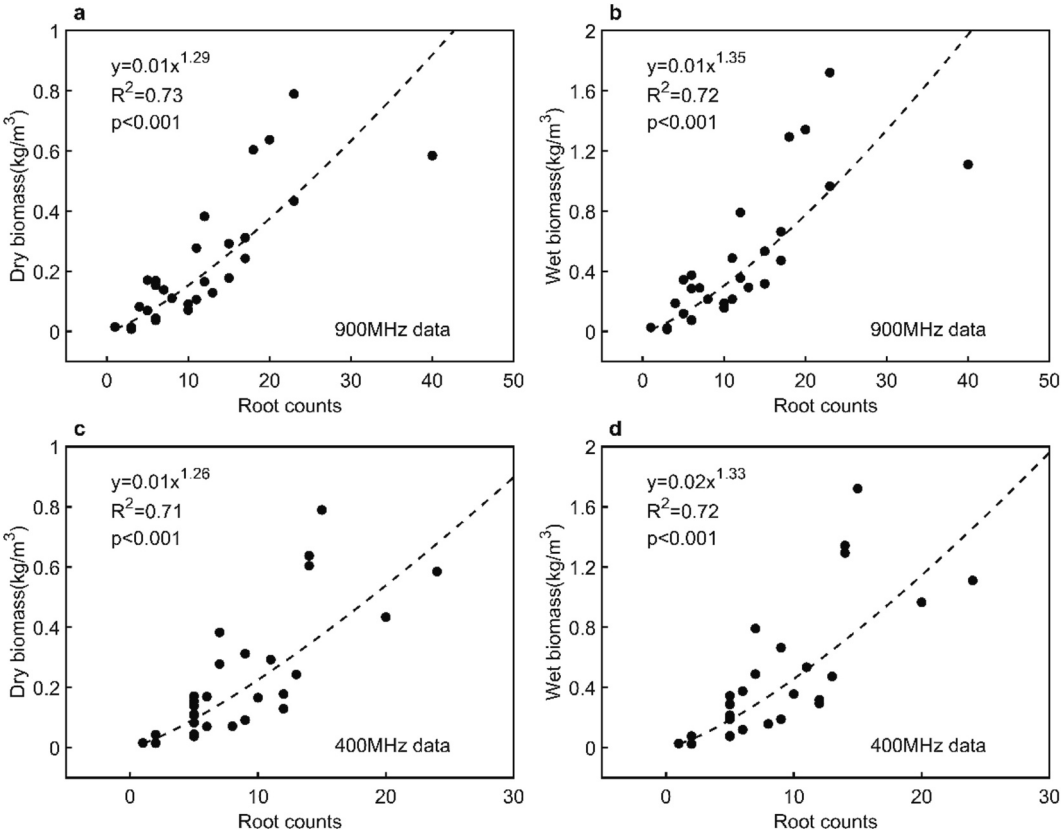

Fig. 9. Relationships of root counts against root biomass **a** detected root counts on 900 MHz radargram vs. dry biomass; **b** detected root counts on 900 MHz radargram vs. wet biomass; **c** detected root counts on 400 MHz radargram vs. dry biomass; **d** detected root counts on 400 MHz radargram vs. wet biomass.

root count data are simple, convenient and easy to obtain. The parameters used in previous studies require additional data processing after root object interpretation (Butnor et al., 2012; Butnor et al., 2016; Cui et al., 2013; Dannoura et al., 2008; Hirano et al., 2009; Molon et al., 2017), which inevitably causes higher uncertainty in root biomass estimation, while these errors can be avoided by utilizing root count data. Moreover, the introduction and use of deep learning methods in GPR data processing have greatly improved the root identification efficiency and accuracy (Li et al., 2022). This can facilitate the automatic and accurate extraction of root counts from the mass of GPR data for root detection in large areas. Therefore, the proposed method is not only helpful to increase the sampling efficiency and reduce the uncertainty in a wider range of shrub root biomass estimation but also helpful to obtain the root biomass spatial distribution through the location of roots obtained by the GPR. This is important for measuring the belowground competition and determining the location of soil resources available to shrubs.

Root biomass has a significant impact on crucial ecosystem processes, including soil carbon storage, water cycling, and nutrient uptake (Lynch, 1995). Due to the significance of root counts, the proposed method extends the application range of GPR and contributes to the research in a wide range of ecological issues, such as monitoring shrub encroachment in grasslands, assessing forest carbon stocks, and the impact of root systems on soil and water conservation. Furthermore, the method provides a novel and effective means of assessing root biomass at larger scales, and has the potential to be used to predict the response of root system to climate change. This could provide important insights into our understanding of shrub adaptation strategies and knowledge of key ecosystem functions.

4.2. Function of the proxy radius

The proxy radius R_a proposed in this paper, although a hypothetical parameter, has a similar physiological meaning in terms of the theoretical definition as the DBH and the cross-sectional area of the stem in the pipe model used in forestry (Shinozaki et al., 1964b). Traditionally, the DBH is used to estimate the tree aboveground biomass, mainly because of the apparent power-law relationship between these quantities (Ali and Yan, 2017; Pérez Cordero and Kanninen, 2003), while proxy radius R_a also shows a power-law relationship with the root biomass (Fig. 7). Stem cross-sectional area is firstly proposed to estimate the leaf mass of trees based on the pipe model theory (Shinozaki et al., 1964a). The important concept in the pipe model is 'a unit amount of leaves is provided with a pipe whose thickness or cross-sectional area is constant. The pipe runs from the leaves to the stem base through all of the intervening strata. Many pipes are bundled to form a tree' (Shinozaki et al., 1964a). Proxy radius R_a is proposed based on a similar assumption. A unit amount of roots is provided with a pipe. Pipes are bundled to form a root. Roots are bundled to represent a profile. Therefore, the proposed proxy radius R_a could explain the relationship between shrub root biomass and root counts as a bridge. The DBH and stem cross-section area have also been used to estimate the root biomass of trees in some previous studies (Brassard et al., 2011; Medrano-Meraz et al., 2021; Pagès et al., 2004; Salas et al., 2004). However, it is particularly difficult to estimate the root biomass of shrubs by using this type of parameter because of the lack of a well-defined main stem. Here, the proposed proxy radius R_a is expected to solve the difficult problem of shrub root biomass estimation.

4.3. Optimization of the model

Models based on GPR data tend to be inferior to models based on

measured data in the same circumstances. The main reason is that the GPR misses a proportion of roots that exhibit unfavorable detection diameters, angles, and depths or are closely spaced and cannot be singularly detected (Hirano et al., 2009; Liu et al., 2018a; Tanikawa et al., 2013; Tanikawa et al., 2021; Wang et al., 2020). Since the root count is positively correlated with the root abundance belowground, it is inferred that the estimation accuracy of the model is related to the GPR detection rate. Therefore, it may be possible to improve the model accuracy by using the radar detection rate as a correction factor to compensate for any roots not detected by the GPR. However, it is essential to note that substituting a constant detection rate into the model does not directly improve the models, as the model exhibits a power-law form. One possible idea is to generate a correction factor based on the probability distribution of the detection rate from the measured data and then use this factor to correct the root counts results of the GPR.

In this study, the GPR detection rates for all measured profiles using the 900 and 400 MHz antennas were 78 ± 14 % (mean ± SD, $n = 30$) and 60 ± 16 % (mean ± SD, n = 30), respectively. Thirty detection rates were randomly generated as correction factors based on the above mean and standard deviation mentioned. These correction factors were applied to the GPR profiles, i.e., the root counts identified on the GPR profiles was divided by the correction factors to obtain the corrected root counts. Taking the detection rate into account, the corrected root count is brought into closer alignment with the actual root count, resulting in an enhanced performance of the model. The results are shown in Fig. 10. Compared with the results in Fig. 9, the model goodness-of-fit was improved (R^2 in Fig. 10 is higher than that in Fig. 9), indicating that the model can be further optimized by considering the GPR detection rate. In practical applications, the GPR detection rate can be estimated by local sampling experiments such as soil core extraction and profile excavation.

4.4. Limitations of the method

The effectiveness of the GPR in plant root system research is mainly affected by buried nonroot objects, root orientation, soil properties and antenna frequency, as well as the difference in the dielectric constants between roots and soil (Guo et al., 2013a; Hirano et al., 2009). When using the GPR for root detection in the field, nonroot objects may produce hyperbolic reflections that are similar to those produced by roots and therefore can be misidentified as roots during data interpretation (Butnor et al., 2001). Typically, these objects include rock fragments, concretions, animal burrows, and some stratified or segmented soil layers (Butnor et al., 2001), which may be a source of error in estimating the root biomass using the model, especially in complex soil environments. Previous studies have shown that stones (dimension: 6–20 cm) occurring in the forest soil matrix are rarely detected by the GPR regardless of whether they are isolated or occur in clumps (Lantini et al., 2020; Tanikawa et al., 2021). However, the boulders of stones (dimension: >20 cm) in the soil could interfere with root detection (Vafidis et al., 2017). Therefore, we suggest that the potential impact of the false detection rate needs to be assessed in advance when applying this method in areas with high soil heterogeneity. Theoretically, such errors can be partially eliminated by compensating for the false detection rate. However, our study site exhibits high soil homogeneity, and few nonroot objects were found in the soil in this experiment, so this type of error was not considered in this study.

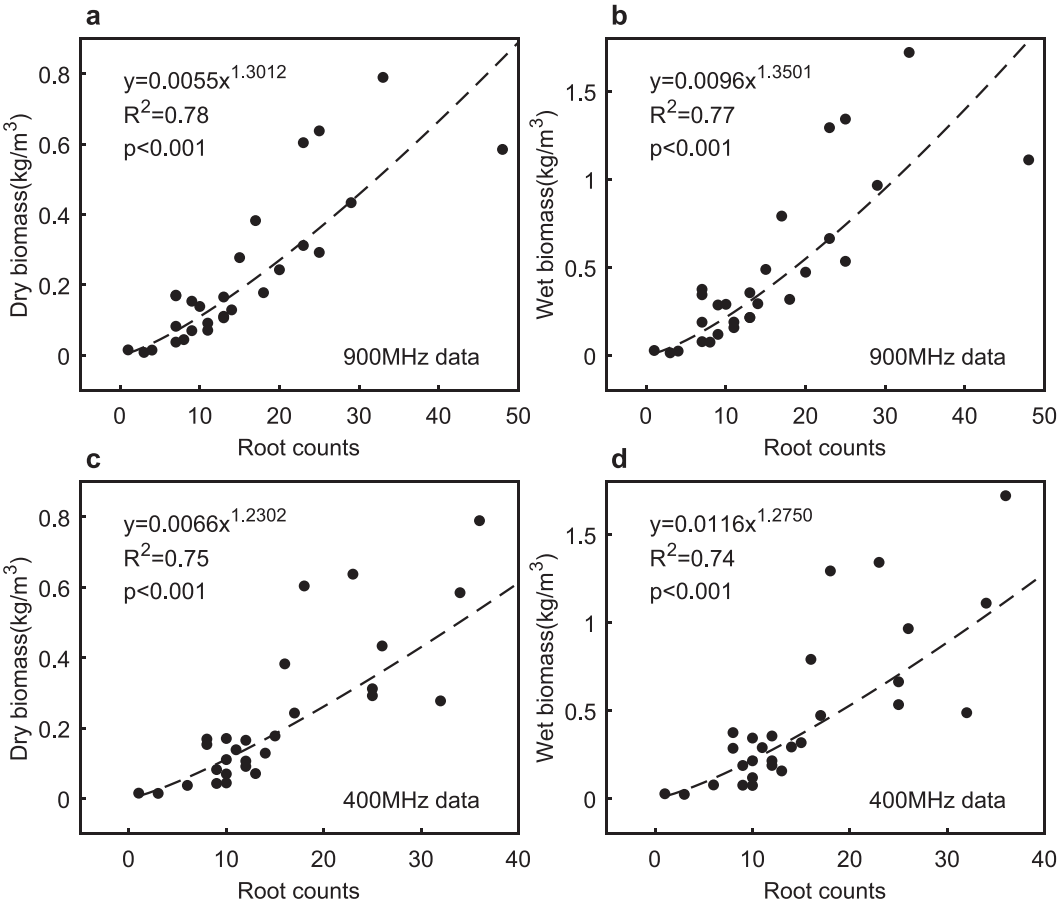

Fig. 10. The corrected results of root biomass estimation of GPR model on **a** 900 MHz frequency for dry biomass; **b** 900 MHz frequency for wet biomass; **c** 400 MHz frequency for dry biomass; **d** 400 MHz frequency for wet biomass.

The root orientation mainly affects the shape of root reflection in radargrams (Guo et al., 2015; Liu et al., 2018a; Tanikawa et al., 2013; Wang et al., 2020; Wu et al., 2014b). When the detection direction of the GPR intersects with the root orientation at an angle of 90°, the reflected root signal shows a clear and standard hyperbolic shape, but when the angle is lower than 45° or higher than 135°, the hyperbolic feature disappears, and it is difficult to identify the root (Tanikawa et al., 2013). When the angle varies between 45° and 135°, the more the angle deviates from 90°, the more severely the hyperbolic shape is deformed, but the root can still be empirically identified using visual interpretation methods (Liu et al., 2018a; Wang et al., 2020). Such signal deformation greatly affects the attribute parameters of roots extracted from A-scan waveforms and B-scan images but slightly affects the root count (Tanikawa et al., 2013). The experimental data in this study showed that the proportion of root orientation values between 45° and 135° is 89 % (Fig. 6d), and we used a deep learning method to effectively recognize roots in the radargrams (Li et al., 2022). However, considering the workload of excavating soil profiles, we set only one survey line direction for each research object in this experiment, so some roots may be missed. It is suggested that survey lines can be set up in a crisscrossing manner for GPR detection in practical applications to improve the accuracy of root count identification.

The antenna frequency affects the detectable depth and the resolution of roots (Annan, 2009; Barton and Montagu, 2004). High-frequency antennas provide a limited depth penetration but a high spatial resolution, while low-frequency antennas exhibit the opposite (Daniels, 2009). In this study, the two antenna frequencies (900 and 400 MHz) achieve a comparable performance in the biomass estimation model (Fig. 9, Table 3), although they provide different root detection rates (Table 2). The main reason for this result is that the number of roots, as a statistic magnitude, represents the overall level of the root biomass across the radar profile and can tolerate a certain degree of error due to the different identification rates at the different antenna frequencies of the GPR. However, we only collected data at two frequencies in our experiments, and the applicability of the proposed method to the range of GPR detection rate variations needs to be tested with GPR data obtained at higher or lower frequencies. The GPR detection rate in this study is slightly higher than that of Hirano et al. (2012) with similar root diameter distribution. This may be related to the experimental environment, plant species, roots identified method and the type of GPR used.

In addition, the limitations of the methodology itself are manifested in three ways. Firstly, the quantitative relationship between proxy radius R_a and the root biomass may vary for different species, so the proposed method needs to be calibrated for different species in practical applications. The method has a theoretical assumption that the density ρ of coarse roots of different diameters is the same, which is applicable to the coarse roots of the shrubs in this study. However, for the coarse roots of trees in forests with a wide range of diameters (e.g., from 0.2 cm to 20 cm), it is likely that the root densities also vary considerably, and thus the reasonableness of this assumption needs to be further verified. So, the method needs to be improved when applied it to the estimation of root biomass in forest trees. One possible suggestion is to analyze the variation in root density by collecting samples of coarse roots of different diameters to find the relationship between root density and root diameter. On this basis, the coefficient k in Eq. (3) should be redesigned and adjusted. Shrubs in arid and semiarid regions are probably the most appropriate due to their low root density and wide-ranging root systems. Secondly, this method summarizes the coarse lateral root biomass but cannot characterize taproots or below-stump mass directly underneath the shrub. Given the complexity of plant species and root conditions, there is a need to optimize the experimental design and develop advanced data processing algorithms to further expand the application of the GPR in plant root research. Finally, the proposed method focuses on estimating the total root biomass within a given area. Compared to existing methods, which are capable of estimating the root biomass or diameter for individual root, the method has limitations in accurately determining individual root biomass.

5. Conclusion

In this work, we present a simple and effective method for estimating the coarse lateral root biomass of shrubs by constructing a quantitative relationship between the root counts detected by the GPR and the excavated root biomass in the radar profile. The proxy radius R_a proposed in this work is an effective parameter to characterize the total biomass of all roots in the corresponding soil volume ($R^2 > 0.9$, Fig. 7). When using the proxy radius to estimate root biomass, its role may be analogous to using DBH to estimate above-ground biomass in trees. How to obtain and further apply this parameter requires further exploration in practice. The proposed model achieves satisfactory accuracy in estimating the coarse lateral root biomass of shrubs, whether using measured data ($R^2 > 0.82$, Fig. 8) or GPR data (900 MHz: $R^2 > 0.72$, 400 MHz: $R^2 > 0.71$, Fig. 9), opening doors for regional-scale assessments of shrub communities' belowground carbon stocks. This advancement has the potential to transform how we monitor carbon storage and inform strategies for mitigating climate change. For instance, policymakers could leverage this approach to prioritize conservation efforts in areas with high carbon sequestration potential. Additionally, it can inform studies on root-soil interactions, linking root systems to soil health, water conservation, and ecosystem resilience. This knowledge empowers researchers and conservationists to develop strategies for maintaining healthy ecosystems in the face of environmental challenges. We recommend further research to validate the model in diverse ecosystems, particularly forest ecosystems, and explore its integration with other tools for comprehensive belowground assessments.

CRediT authorship contribution statement

Luyun Zhang: Writing – original draft, Validation, Software, Methodology. **Zheng Zhang:** Writing – original draft, Visualization, Methodology. **Li Guo:** Writing – review & editing, Supervision. **Xihong Cui:** Writing – review & editing, Supervision, Funding acquisition, Conceptualization. **John R. Butnor:** Writing – review & editing, Supervision. **Shupeng Li:** Supervision, Resources, Investigation. **Xin Cao:** Supervision. **Xuehong Chen:** Supervision.

Declaration of competing interest

The authors declare that they have no known competing financial interests or personal relationships that could have appeared to influence the work reported in this paper.

Data availability

Data will be made available on request.

Acknowledgements

This study was supported by the National Natural Science Foundation of China (Grant No. 42271329). The authors are thankful for the assistance in field data collection from Xinbo Liu, Zhenxian Quan, Yunze Zang, Jiahao Wen, jinfeng Shi. We also thank two anonymous reviewers and two editor (Paola Verlicchi and Qinxue Wang) for their valuable comments and suggestions, which have helped improve the quality of this paper.

References

Addo-Danso, S.D., Prescott, C.E., Smith, A.R., 2016. Methods for estimating root biomass and production in forest and woodland ecosystem carbon studies: a review. For. Ecol. Manage. 359, 332–351.

Alamusa, Jiang D.M., Pei, T.F., 2003. Relationship between root system distribution and soil moisture of artificial Caragana icrophylla vegetation in sandy land. J. Soil Water Conserv. 17, 78–81.

Alani, A.M., Lantini, L., 2019. Recent advances in tree root mapping and assessment using non-destructive testing methods: a focus on ground penetrating radar. Surv. Geophys. 41, 605–646.

Ali, A., Yan, E.R., 2017. The forest strata-dependent relationship between biodiversity and aboveground biomass within a subtropical forest. For. Ecol. Manage. 401, 125–134.

Annan, A.P., 2009. Chapter 1 - electromagnetic principles of ground penetrating radar. In: Jol, H.M. (Ed.), Ground Penetrating Radar Theory and Applications. Elsevier, Amsterdam, pp. 1–40.

Bain, J.C., Day, F.P., Butnor, J.R., 2017. Experimental evaluation of several key factors affecting root biomass estimation by 1500 MHz ground-penetrating radar. Remote Sens. (Basel) 9, 1337.

Barton, C.V.M., Montagu, K.D., 2004. Detection of tree roots and determination of root diameters by ground penetrating radar under optimal conditions. Tree Physiol. 24, 1323–1331.

Bartos, D.L., Sims, P.L., 1974. Root dynamics of a shortgrass ecosystem. J. Range Manage. 27, 33–36.

Baumann, G., 2009. How to Assess Rangeland Condition in Semiarid Ecosystems? The Indicative Value of Vegetation in the High Atlas Mountains. Morocco. Universität zu Köln, Cologne, Germany.

Bi, L., Xing, L., Liang, H., Lin, J., 2023. Estimation of coarse root system diameter based on ground-penetrating radar forward modeling. Forests 14, 1370.

Brassard, B.W., Chen, H.Y.H., Bergeron, Y., Pare, D., 2011. Coarse root biomass allometric equations for Abies balsamea, Picea mariana, Pinus banksiana, and Populus tremuloides in the boreal forest of Ontario. Canada. Biomass Bioenergy 35, 4189–4196.

Brovkin, V., Boysen, L., Arora, V.K., Boisier, J.P., Cadule, P., Chini, L., et al., 2013. Effect of anthropogenic land-use and land-cover changes on climate and land carbon storage in CMIP5 projections for the twenty-first century. J. Climate 26, 6859–6881.

Butnor, J.R., Doolittle, J.A., Kress, L., Cohen, S., Johnsen, K.H., 2001. Use of ground-penetrating radar to study tree roots in the southeastern United States. Tree Physiol. 21, 1269–1278.

Butnor, J.R., Doolittle, J.A., Johnsen, K.H., Samuelson, L., Stokes, T., Kress, L., 2003. Utility of ground-penetrating radar as a root biomass survey tool in forest systems. Soil Sci. Soc. Am. J. 67, 1607–1615.

Butnor, J.R., Barton, C., Day, F.P., Johnsen, K.H., Mucciardi, A.N., Schroeder, R., et al., 2012. Using Ground-Penetrating Radar to Detect Tree Roots and Estimate Biomass. Berlin Heidelberg, Measuring Roots. Springer, pp. 213–245.

Butnor, J.R., Samuelson, L.J., Stokes, T.A., Johnsen, K.H., Anderson, P.H., González-Benecke, C.A., 2016. Surface-based GPR underestimates below-stump root biomass. Plant and Soil 402, 47–62.

Canadell, J., Jackson, R.B., Ehleringer, J.B., Mooney, H.A., Sala, O.E., Schulze, E.D., 1996. Maximum rooting depth of vegetation types at the global scale. Oecologia 108, 583–595.

Cao, C., Jiang, D., Luo, Y., Kou, Z., 2004. Stability of Caragana microphylla plantation for wind protection and sand fixation. Acta Ecol. Sin. 24, 1178–1186.

Cao, X., Liu, Y., Liu, Q., Cui, X., Chen, X., Chen, J., 2018. Estimating the age and population structure of encroaching shrubs in arid/semiarid grasslands using high spatial resolution remote sensing imagery. Remote Sens. Environ. 216, 572–585.

Čermák, J., Hruška, J., Martinková, M., Prax, A., 2000. Urban tree root systems and their survival near houses analyzed using ground penetrating radar and sap flow techniques. Plant and Soil 219, 103–116.

Chopart, J.-L., Sine, B., Dao, A., Muller, B., 2008. Root orientation of four sorghum cultivars: application to estimate root length density from root counts in soil profiles. Plant Root 2, 67–75.

Cox, K.D., Scherm, H., Serman, N., 2005. Ground-penetrating radar to detect and quantify residual root fragments following peach orchard clearing. Horttechnology 15, 600–607.

Cui, X., Chen, J., Shen, J., Cao, X., Chen, X., Zhu, X., 2011. Modeling tree root diameter and biomass by ground-penetrating radar. Science China Earth Sciences 54, 711–719.

Cui, X., Liu, X., Cao, X., Fan, B., Zhang, Z., Chen, J., et al., 2019. Pairing dual-frequency GPR in summer and winter enhances the detection and mapping of coarse roots in the semi-arid shrubland in China. Eur. J. Soil Sci. 71, 236–251.

Cui, X.H., Guo, L., Chen, J., Chen, X.H., Zhu, X.L., 2013. Estimating tree-root biomass in different depths using ground-penetrating radar: evidence from a controlled experiment. IEEE Trans. Geosci. Remote Sens. 51, 3410–3423.

Daniels, D.J., 2004. Ground Penetrating Radar. Institution of Electrical Engineers, London.

Daniels, D.J., 2009. Chapter 4 - Antennas. In: Jol, H.M. (Ed.), Ground Penetrating Radar Theory and Applications. Elsevier, Amsterdam, pp. 99–139.

Dannoura, M., Hirano, Y., Igarashi, T., Ishii, M., Aono, K., Yamase, K., et al., 2008. Detection of Cryptomeria japonica roots with ground penetrating radar. Plant Biosyst 142, 375–380.

Dean, C., Kirkpatrick, J.B., Harper, R.J., Eldridge, D.J., 2015. Optimising carbon sequestration in arid and semiarid rangelands. Ecol. Eng. 74, 148–163.

Freschet, G.T., Pagès, L., Iversen, C.M., Comas, L.H., Rewald, B., Roumet, C., et al., 2021. A starting guide to root ecology: strengthening ecological concepts and standardising root classification, sampling, processing and trait measurements. New Phytol. 232, 973–1122.

Geisser, S., 1974. A predictive approach to the random effect model. Biometrika 61, 101–107.

Grote, K., Hubbard, S., Rubin, Y., 2003. Field-scale estimation of volumetric water content using ground-penetrating radar ground wave techniques. Water Resour. Res. 39, 14.

Guo, L., Chen, J., Cui, X.H., Fan, B.H., Lin, H., 2013a. Application of ground penetrating radar for coarse root detection and quantification: a review. Plant and Soil 362, 1–23.

Guo, L., Lin, H., Fan, B.H., Cui, X.H., Chen, J., 2013b. Impact of root water content on root biomass estimation using ground penetrating radar: evidence from forward simulations and field controlled experiments. Plant and Soil 371, 503–520.

Guo, L., Wu, Y., Chen, J., Hirano, Y., Tanikawa, T., Li, W.T., et al., 2015. Calibrating the impact of root orientation on root quantification using ground-penetrating radar. Plant and Soil 395, 289–305.

He, J., 2012. Precipitation variation characteristics of Xilinhot city for 50 years. Chin. Agri. Sci. Bull. 28, 271–278.

Hirano, Y., Dannoura, M., Aono, K., Igarashi, T., Ishii, M., Yamase, K., et al., 2009. Limiting factors in the detection of tree roots using ground-penetrating radar. Plant and Soil 319, 15–24.

Hirano, Y., Yamamoto, R., Dannoura, M., Aono, K., Igarashi, T., Ishii, M., et al., 2012. Detection frequency of Pinus thunbergii roots by ground-penetrating radar is related to root biomass. Plant and Soil 360, 363–373.

Hruska, J., Cermak, J., Sustek, S., 1999. Mapping tree root systems with ground-penetrating radar. Tree Physiol. 19, 125–130.

Hu, X., Li, X.-Y., Guo, L.-L., Liu, Y., Wang, P., Zhao, Y.-D., et al., 2019. Influence of shrub roots on soil macropores using X-ray computed tomography in a shrub-encroached grassland in northern China. J. Soil. Sediment. 19, 1970–1980.

Huber, E., Hans, G., 2018. RGPR—An open-source package to process and visualize GPR data. In: 2018 17th International Conference on Ground Penetrating Radar (GPR). IEEE, pp. 1–4.

Huisman, J.A., Hubbard, S.S., Redman, J.D., Annan, A.P., 2003. Measuring soil water content with ground penetrating radar: a review. Vadose Zone J. 2, 476–491.

Lantini, L., Tosti, F., Giannakis, I., Zou, L., Benedetto, A., Alani, A.M., 2020. An enhanced data processing framework for mapping tree root systems using ground penetrating radar. Remote Sens. (Basel) 12, 3417.

Li, S.P., Cui, X.H., Guo, L., Zhang, L.Y., Chen, X.H., Cao, X., 2022. Enhanced automatic root recognition and localization in GPR images through a yolov4-based deep learning approach. IEEE Trans. Geosci. Remote Sens. 60, 14.

Li, W.T., Cui, X.H., Guo, L., Chen, J., Chen, X.H., Cao, X., 2016. Tree root automatic recognition in ground penetrating radar profiles based on randomized Hough transform. Remote Sens. (Basel) 8, 430.

Li, X.Y., Zhang, S.Y., Peng, H.Y., Hu, X., Ma, Y.J., 2013. Soil water and temperature dynamics in shrub-encroached grasslands and climatic implications: results from Inner Mongolia steppe ecosystem of North China. Agric. For. Meteorol. 171, 20–30.

Liang, H., Fan, G., Li, Y., Zhao, Y., 2021. Theoretical development of plant root diameter estimation based on GprMax data and neural network modelling. Forests 12, 615.

Liu, A.X., Liu, Z.J., Wang, C.Y., Niu, Z., Yan, D.M., 2003. Monitoring of desertification in Central Asia and western China using long term NOAA-AVHRR NDVI time-series data. International Geoscience and Remote Sensing Symposium (IGARSS). 4, 2278–2280.

Liu, Q., Cui, X., Liu, X., Chen, J., Chen, X., Cao, X., 2018a. Detection of root orientation using ground-penetrating radar. IEEE Trans. Geosci. Remote Sens. 56, 93–104.

Liu, X., Dong, X., Xue, Q., Leskovar, D.I., Jifon, J., Butnor, J.R., et al., 2018b. Ground penetrating radar (GPR) detects fine roots of agricultural crops in the field. Plant and Soil 423, 517–531.

Liu, X., Cui, X., Guo, L., Chen, J., Li, W., Yang, D., et al., 2019. Non-invasive estimation of root zone soil moisture from coarse root reflections in ground-penetrating radar images. Plant and Soil 436, 623–639.

Lynch, J., 1995. Root architecture and plant productivity. Plant Physiol. 109, 7–13.

Medrano-Meraz, F., López-López, M., Ángeles-Pérez, G., Cobos, F., Jong, B., 2021. Allometric equations for belowground biomass and carbon content of pinus patula schl. Et Cham. Rev. Fitotec. Mex. 44, 443.

Miao, H.X., Chen, S.P., Chen, J.Q., Zhang, W.L., Zhang, P., Wei, L., et al., 2009. Cultivation and grazing altered evapotranspiration and dynamics in Inner Mongolia steppes. Agric. For. Meteorol. 149, 1810–1819.

Molon, M., Boyce, J.I., Arain, M.A., 2017. Quantitative, nondestructive estimates of coarse root biomass in a temperate pine forest using 3-D ground-penetrating radar (GPR). Eur. J. Vasc. Endovasc. Surg. 122, 80–102.

Pagès, L., Vercambre, G., Drouet, J.-L., Lecompte, F., Collet, C., Le Bot, J., 2004. Root Typ: a generic model to depict and analyse the root system architecture. Plant and Soil 258, 103–119.

Pérez Cordero, L.D., Kanninen, M., 2003. Aboveground biomass of Tectona grandis plantations in Costa Rica. J. Trop. For. Sci. 15, 199–213.

Plaza-Bonilla, D., Alvaro-Fuentes, J., Hansen, N.C., Lampurlanes, J., Cantero-Martinez, C., 2014. Winter cereal root growth and aboveground-belowground biomass ratios as affected by site and tillage system in dryland Mediterranean conditions. Plant and Soil 374, 925–939.

R Core Team, 2022. R: A Language and Environment for Statistical Computing. R Foundation for Statistical Computing, Vienna, Austria.

Raich, J.W., Nadelhoffer, K.J., 1989. Belowground carbon allocation in forest ecosystems - global trends. Ecology 70, 1346–1354.

Salas, E., Ozier-Lafontaine, H., Nygren, P., 2004. A fractal root model applied for estimating the root biomass and architecture in two tropical legume tree species. Ann. For. Sci. 61, 337–345.

Samuelson, L.J., Stokes, T.A., Butnor, J.R., Johnsen, K.H., Gonzalez-Benecke, C.A., Anderson, P., et al., 2014. Ecosystem carbon stocks in Pinus palustris forests. Can. J. For. Res. 44, 476–486.
Samuelson, L.J., Stokes, T.A., Butnor, J.R., Johnsen, K.H., Gonzalez-Benecke, C.A., Martin, T.A., et al., 2017. Ecosystem carbon density and allocation across a chronosequence of longleaf pine forests. Ecol. Appl. 27, 244–259.
Schafer, W.M., Nielsen, G.A., 1981. Root biomass calculation using a modified counting technique. J. Range Manage. 34, 245–247.
Shinozaki, K., Yoda, K., Hozumi, K., Kira, T., 1964a. A quantitative analysis of plant form-the pipe model theory: I. Basic analyses. Japanese J. Ecol. 14, 97–105.
Shinozaki K, Yoda K, Hozumi K, Kira T. A quantitative analysis of plant form-the pipe model theory: II. Further evidence of the theory and its application in forest ecology. Japanese J. Ecol. 1964b; 14: 133–139.
Sjoholm, H., Reynders, M., Ffolliott, P., Ben, Salem B., 1989. Arid Zone Forestry; a Guide for Field Technicians. FAO, Roma (Italia).
Stokes, A., Fourcaud, T., Hruska, J., Cermák, J., Nadyezdhina, N., Nadyezhdin, V., et al., 2002. An evaluation of different methods to investigate root system architecture of urban trees in situ: I. Ground-penetrating radar. J. Arboric. 28, 2–10.
Stover, D.B., Day, L.F., Butnor, J.R., Drake, B.G., 2007. Effect of elevated CO2 on coarse-root biomass in Florida scrub detected by ground-penetrating radar. Ecology 88, 1328–1334.
Sun, D., Jiang, F., Wu, H., Liu, S., Luo, P., Zhao, Z., 2023. Root location and root diameter estimation of trees based on deep learning and ground-penetrating radar. Agronomy 13, 344.
Tanikawa, T., Hirano, Y., Dannoura, M., Yamase, K., Aono, K., Ishii, M., et al., 2013. Root orientation can affect detection accuracy of ground-penetrating radar. Plant and Soil 373, 317–327.
Tanikawa, T., Ikeno, H., Yamase, K., Dannoura, M., Aono, K., Hirano, Y., 2021. Can ground-penetrating radar detect adjacent roots and rock fragments in forest soil? Plant and Soil 468, 239–257.
Vafidis, A., Economou, N., Kritikakis, G., Galetakis, M., Vasiliou, A., Apostolopoulos, G., et al., 2017. Imaging Boulders Using the Ground Penetrating Radar (GPR) Method. Bearing Capacity of Roads, Railways and Airfields. CRC Press, pp. 1567–1572.
Wang, J., Liu, M., Sheng, S., Xu, C., Liu, X., Wang, H., 2008. Spatial distributions of soil water, salts and roots in an arid arbor-herb community. Acta Ecol. Sin. 28, 4120–4127.
Wang, M.K., Wen, J., Li, W.B., 2020. Qualitative research: the impact of root orientation on coarse roots detection using ground-penetrating radar (GPR). BioResources 15, 2237–2257.
WRB IWG, 2006. World Reference Base for Soil Resources 2006. World soil resources reports no.103.. FAO, Rome.
Wu, Y., Guo, L., Cui, X.H., Chen, J., Cao, X., Lin, H., 2014a. Ground-penetrating radar-based automatic reconstruction of three-dimensional coarse root system architecture. Plant and Soil 383, 155–172.
Wu, Y., Guo, L., Li, W.T., Cui, X.H., Chen, J., 2014b. Comment on: “root orientation can affect detection accuracy of ground-penetrating radar”. Plant and Soil 380, 441–444.
Yamase, K., Tanikawa, T., Dannoura, M., Ohashi, M., Todo, C., Ikeno, H., et al., 2018. Ground-penetrating radar estimates of tree root diameter and distribution under field conditions. Trees 32, 1657–1668.
Yiruhan, Ailikun, Ma, Z.G., Shiyomi, M., 2011. Forty-eight-year climatology of air temperature and precipitation changes in Xilinhot, Xilingol steppe (Inner Mongolia). China. Grassl Sci 57, 168–172.
Zhao, Y., Peth, S., Wang, X.Y., Lin, H., Horn, R., 2010. Controls of surface soil moisture spatial patterns and their temporal stability in a semi-arid steppe. Hydrol. Process. 24, 2507–2519.
Zhou, Y., Singh, J., Butnor, J.R., Coetsee, C., Boucher, P.B., Case, M.F., et al., 2022. Limited increases in savanna carbon stocks over decades of fire suppression. Nature 603, 445–449.
Zhu, S., Huang, C., Su, Y., Sato, M., 2014. 3D ground penetrating radar to detect tree roots and estimate root biomass in the field. Remote Sens. (Basel) 6, 5754–5773.